Viscoelasticity of reversibly crosslinked networks of semiflexible polymers

Jan Plagge,* Andreas Fischer, and Claus Heussinger
Institute for Theoretical Physics, Georg-August University of Göttingen, Friedrich-Hund Platz 1, 37077 Göttingen, Germany
(Received 12 February 2016; revised manuscript received 3 June 2016; published 27 June 2016)

We present a theoretical framework for the linear and nonlinear viscoelastic properties of reversibly crosslinked networks of semiflexible polymers. In contrast to affine models where network strain couples to the polymer end-to-end distance, in our model strain rather serves to locally distort the network structure. This induces bending modes in the polymer filaments, the properties of which are slaved to the surrounding network structure. Specifically, we investigate the frequency-dependent linear rheology, in particular in combination with crosslink binding-unbinding processes. We also develop schematic extensions to describe the nonlinear response during creep measurements as well as during constant strain-rate ramps.

DOI: 10.1103/PhysRevE.93.062502

I. INTRODUCTION

The cytoskeleton is a viscoelastic material with many interesting mechanical behaviors. From a theoretical point of view these systems are viewed as networks of reversibly (or permanently) crosslinked semiflexible polymers [1–3]. Over the years many theoretical works have discovered and partially explained different regimes, where certain components of the networks dominate the mechanical response [4–9]. Simulations on simplified model systems provide a helpful alternative approach to study the pertinent problems [10–16].

Most notably, the affine approach, relying on the nonlinear polymer force-extension relation [17,18], has allowed to rationalize many of the diverse experimental findings. Recent advances include the glassy wormlike chain model [19], effective medium theories [20–22], as well as models that use analogies with rigidity percolation [23], the jamming transition in dense particle packings [24], and its concept of "soft modes." This latter analogy [25,26] is based on the fact that densly packed hard particles prefer to rotate around—instead of press into each other. After all, hard particles are "incompressible." Similarly, semiflexible polymers are nearly inextensible, and under deformation they prefer to deform perpendicular to the polymer axis—what is commonly understood as *bending*.

Here, we present a theoretical framework that is entirely constructed on the basis of these bending deformations. The force-extension relation does not play a role for the linear response of the network. The theory is based on results [25] on the static linear elasticity. The key achievement of the present work is that it generalizes these results to finite frequencies, allowing us to calculate the linear elastic and viscous moduli over the whole frequency regime relevant for standard rheological experiments.

The paper is structured as follows: First a brief review of the static modulus is given (Sec. II). Then (Sec. III) the model is generalized to finite frequencies. In Sec. IV low-frequency crosslink binding processes are considered, and, finally (Sec. V), we discuss possible nonlinear rheological effects presenting schematic extensions of the linear model.

II. REVIEW: STATIC MODULUS

We will consider the properties of a test filament crosslinked into a network of other filaments. The filament is described in terms of the wormlike chain model. In the "weakly bending" approximation the bending energy of the filament can be written as

$$H_b = \frac{\kappa_b}{2}\int_0^L \left(\frac{\partial^2 y}{\partial s^2}\right)^2 ds, \tag{1}$$

where κ_b is the filament bending stiffness and $y(s)$ is the transverse deflection of the filament from its (straight) reference configuration at $y_0(s) = 0$. In these expressions s is the arclength, $s = [0, L]$, and L is the length of the filament.

The effect of the surrounding network is to confine the test filament to a tubelike region in space. In this way the actual network is substituted by an effective potential that acts on the test filament. A convenient potential is the harmonic tube

$$V = \frac{1}{2}\int_0^L k(s)(y(s) - \bar{y}(s))^2 ds, \tag{2}$$

where $k(s)$ is the strength of the confinement and $\bar{y}(s)$ is the tube center, which may or may not differ from the reference configuration $y_0(s)$ of the filament.

A key assumption in our model is that the tube depends on network strain γ. In particular, we will assume that the tube centerline follows the strain γ,

$$\bar{y}(s,\gamma) = \beta(s)\gamma L, \tag{3}$$

with a shape function $\beta(s)$ that is slaved to the local network structure. The occurrence of the filament length L signifies its role as nonaffinity length, up to which network response is nonaffine and determined by local structural features. Such a scaling has been observed in the simulations of Ref. [27]. Theoretically, one can derive it from the assumption of affine motion for the *filament centers of mass* [25]. In this picture, viscous stresses of the solvent drag along entire filament patches of length L, however, without stretching them. Because filaments are connected to their neighbors such motion necessarily leads to local network distortions which are captured by the shape functions β.

The physical picture of strain-induced local deformations is thus that by straining the network the preferred location (the tube) of a polymer changes—and not primarily the

*Current address: Deutsches Institut für Kautschuktechnologie, e. V., Eupener Str. 33, 30519 Hannover, Germany.

polymer itself. This is the key difference to many previous works that assume strain to lead to a change in end-to-end distance of the polymers. The rheology in these models then is a direct consequence of the force-extension relation of the single polymer. By way of contrast, in our approach, the force-extension relation plays no role at all (for the linear response), and the polymers can be taken to be completely inextensible. In fact, one can show [25] that tube deformations leave the end-to-end distance (to linear order) unchanged, as long as one takes for the shape function $\beta_i \equiv \beta(s_i) = -\cot\theta_i$ at crosslink position s_i, where θ_i is the angle at which the crosslinked filament connects to the test filament. In this way, the polymer tube changes in such a way as to guarantee that the polymer end-to-end distance is *not* changed under network straining (in linear response) (see Fig. 1). For any real filament this assumption of inextensibility breaks down at the point, where the relevant forces become large enough to compete with the extensional stiffness. This may happen, for example, in nonlinear response (see Sec. V) or at high-enough frequencies where viscous stresses in the medium enforce affine motion.

We assume the network to be represented by an effective medium that couples to the test filament only at the crosslinking points,

$$k(s) = k_m \sum_{i=1}^{N} \alpha_i \delta(s - s_i), \tag{4}$$

where N is the total number of crosslinking sites, and k_m represents the stiffness of the medium. This is expected to be rather uniform, hence having roughly the same elastic properties at every crosslink. The effects of local variability, e.g., binding angle, is accounted for by the factors $\alpha_i = \sin^2\theta_i$. There may be cases where k_m may actually vary from point to point. For example, in composite networks of two or more filaments (e.g., actin and microtubules) one has to differentiate between couplings given that the test filament is of either type. Such a scenario has been dealt with in Ref. [28].

The central goal of this work is to calculate in a self-consistent way the stiffness k_m, as well as its frequency-dependent generalization, the complex modulus $g^\star(\omega)$. In previous work [25] we have argued that the stiffness may be calculated from the equation

$$\tfrac{1}{2}k_m(\gamma L)^2 = \left\langle \min_{y(s)}(H_b[y] + V[y](k_m)) \right\rangle, \tag{5}$$

where the angular brackets denote ensemble average with respect to the quenched local network structure. This equation highlights the twofold role of the stiffness k_m. On a mesoscopic scale it is defined as an elastic modulus that quantifies the energy cost to deformation (left-hand side). On a microscopic scale (right-hand side) this deformation is carried by filaments that are themselves connected to the elastic medium via the crosslinks (also see Fig. 2).

Formally, Eq. (5) represents a Cayley-tree approximation to the real network, that is, loops of filaments are neglected. This allows to spread a network strain from one filament via its crosslinks to its neighboring filaments and further on to secondary and tertiary neighbors. Continuing this process to infinity one obtains a self-consistent equation similar to a classic Dyson equation.

Equation (5) can be solved in a simplified scaling picture by assuming a single wavelength $\lambda = L/N$ and one angle θ to dominate (see the Appendix for details)

$$k_m \sim \kappa N^3(N - N_c), \tag{6}$$

where we defined $N_c = 1/\alpha_i\beta_i^2$, which represents the percolation threshold of the model. The modulus is zero if fewer than N_c crosslinks are present and scales linearly with δN in the critical regime. As explained above, our theory can be taken as a Cayley tree approximation to the real network. The percolation threshold therefore is the one of the Cayley tree. Therefore it is not surprising that its location, as well as its exponents are different from Maxwell counting or exact values [29,30]. Nevertheless, the very presence of such a "liquid-solid" transition, which is a genuine property of real filament networks, allows us to study both sides and monitor the viscoelastic properties when crossing the transition (see below).

Far above the threshold Eq. (6) indicates that the modulus scales with $\sim N^4$. We have shown previously [25] how the inclusion of different wavelengths as well as angles can change the scaling of the modulus with crosslink concentration N (also see Fig. 7).

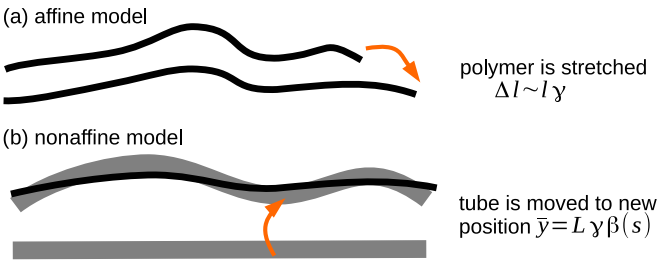

FIG. 1. Illustration of the differences between our (nonaffine) model and the affine model of polymer stretching. In the affine model a network strain γ leads to the stretching of a polymer segment (of length l) by $\Delta l \propto \gamma l$. In the nonaffine model we assume that network strain primarily affects the polymer tube, which is deflected to a new position $\bar{y}(s) = L\gamma\beta(s)$. The shape function $\beta(s)$ is determined by the local network structure, such that the polymer is *not* stretched.

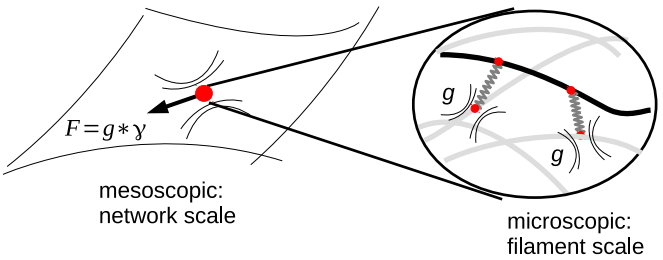

FIG. 2. Illustration of the basic model assumptions. On a mesoscopic scale the network is represented by a continuum viscoelastic body with modulus $g(t)$ (or k_m for the static case). Application of a force F will therefore lead to network strain γ, via the convolution $F(t) = (g \star \gamma)(t)$ (or $k_m \cdot \gamma$). On the microscopic scale the individual filaments couple to the same matrix g (k_m) at their crosslinks. The curved lines enclosing the red dots symbolize this coupling to the viscoelastic matrix.

The static theory presented above has been used in various contexts, e.g., to describe the mixing rule in composite networks of microtubules and f-actin [28]. In the following we want to generalize the theory to account for finite frequency of the deformation, as well as for finite lifetime of the crosslink bond.

III. FINITE FREQUENCY

Experiments are most often conducted in the frequency domain, where a time-dependent oscillatory strain $\gamma(t) = \gamma_0 \sin(\omega t)$ is imposed. In order to account for time-dependent phenomena we first rewrite Eq. (5) as two force-balance equations.

The minimization operation makes the transverse deflection of the polymer, $y(s)$, the solution to the equation

$$0 = \kappa y^{(4)} + \sum_i \delta(s - s_i) T_i \sin\theta_i. \tag{7}$$

Here, we have defined the force in the ith crosslink

$$T_i = k_m \sin\theta_i (y_i - \bar{y}_i). \tag{8}$$

The part of these forces transverse to the polymer ($T_i \sin\theta_i$) must balance the bending force $\kappa y^{(4)}$ to give a stable contour in mechanical equilibrium.

A second balance equation can be obtained by differentiating Eq. (5) with respect to γ. This will give us the force that is needed to displace the polymer by the strain. Using Eq. (5) we find

$$k_m \gamma = \left\langle \sum_{i=1}^{N} T_i \cos\theta_i \right\rangle, \tag{9}$$

where now the forces T_i are projected onto the axis of the fiber. In other words, the external force $F_{\text{ext}} = k_m \gamma$ is balanced by the forces at the n crosslinks.

The generalization to finite frequencies is now straightforward. First, additional viscous (and possibly thermal) forces need to enter the force-balance equations. Second, the stiffness k_m needs to be substituted by a frequency-dependent function $g^\star(\omega)$. This is achieved by defining the response function

$$T(t) = \int_{-\infty}^{t} d\tau g(t-\tau) \frac{\partial \gamma}{\partial \tau} \equiv (g \star \gamma)(t). \tag{10}$$

This function specifies the force at time t that is needed for a given strain history $\gamma(\tau)$.

If $g(t) = k_m$ is constant, then $T = k_m \gamma(t)$, i.e., a quasistatic solid response, while the limit $g(t) = \zeta \delta(t)$ gives a fluidlike behavior, where $T = \zeta \dot{\gamma}$.

With these modifications we obtain the following two equations:

$$\kappa y^{(4)} + \sum_i \alpha_i g \star (y - \bar{y}_i)\delta(s - s_i) = \eta \frac{\partial y}{\partial t} + \xi, \tag{11}$$

$$g \star \gamma + \left\langle \sum_i \alpha_i \beta_i g \star (y - \bar{y}_i) \right\rangle = \eta_z \frac{\partial \gamma}{\partial t} + \xi_z, \tag{12}$$

where η and η_z are drag coefficients governing the viscous forces, while ξ and ξ_z are thermal (random) forces. In the following we will neglect the axial damping η_z (which leads to a high-frequency regime $g^\star \sim \omega$) as well as the noise terms ξ and ξ_z (which can be shown to be subdominant). Equation (11) has to be solved for $y(s,t)$ and used in Eq. (12) to determine the response function $g(t)$ or in frequency-space $g^\star(\omega) = g'(\omega) + ig''(\omega)$. Adopting the latter representation, Eq. (11) can be written as

$$y(x,\omega) = \sum_i \mathcal{G}(x, x_i, \omega) g^\star \alpha_i (y_i - \bar{y}_i), \tag{13}$$

which shows how the Greens function $\mathcal{G}$ mediates between the position x_i of the crosslink, where the force $\hat{T}_i = g^\star \alpha_i (y_i - \bar{y}_i)$ is applied, and the actual position x, at which the deflection is evaluated. The Greens function itself is given as

$$\mathcal{G}_{ij}(\omega) \equiv \mathcal{G}(x_i, x_j, \omega) = \sum_q \frac{\psi_q(x_i)\psi_q^\star(x_j)}{\kappa q^4 + i\omega\eta}, \tag{14}$$

where ψ_q are suitable basis functions, e.g., trigonometric functions that are chosen to respect the boundary conditions.

Inserting into Eq. (12) one obtains the final equation

$$1 = \left\langle \sum_{ij} (1 + g^\star \mathcal{S} G)^{-1}_{ij} \alpha_i \beta_i \beta_j \right\rangle, \tag{15}$$

where we introduced the diagonal matrix $S_{ij} = \alpha_i \delta_{ij}$. Equation (15) needs to be solved numerically for the modulus $g^\star(\omega)$.

The full numerical solution of Eq. (15) is presented in Fig. 3 for various crosslink densities N. For a numerical evaluation we set $\kappa_b = 1$, $L = 1$, thus fixing energy and length scales. The time scale is set by the viscous coefficient $\eta = 1$ of the filaments. The noise ξ and ξ_z turn out to be subdominant. The leading contribution to the modulus is thus athermal and independent of temperature.

On small frequencies the static solution is recovered and leads to a plateau in the storage modulus, $g_0 \sim N^x$, where the value of the exponent x depends on the type of quenched local network structure (angular brackets). This sensitivity on network structure can, for example, be seen in Fig. 7, where the plateau modulus rises by several orders of magnitude just by changing the angle distribution.

Experimentally, the plateau modulus is measured as a function of actin- or crosslink concentration. With additional

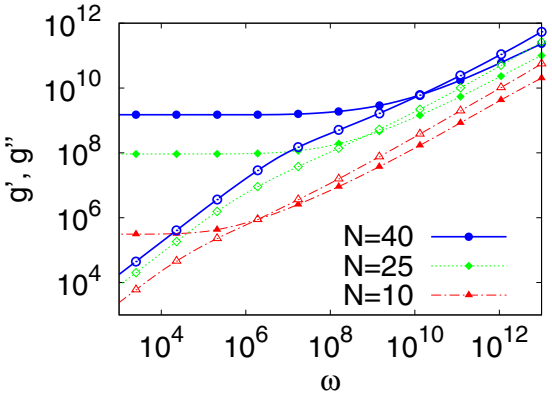

FIG. 3. Frequency-dependent modulus $g^\star = g' + ig''$ for different crosslink number N; storage modulus g' (solid lines and filled symbols); loss modulus g'' (broken lines and open symbols).

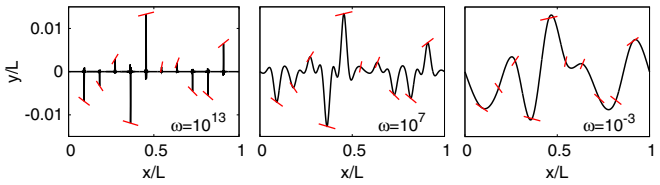

FIG. 4. Amplitude $y_0(\omega)$ of filament contour $y(x,t) = y_0(x)\sin(\omega t)$ for different driving frequencies. For high ω (left) the filament feels the driving only in the vicinity of the crosslinks [represented by the light (red) bars]. Low-frequency driving (right) only excites the longest possible wavelengths, which are set by the local network structure (orientation and distance of contacting filaments).

assumptions on how N depends on the concentration $c_\times$ of crosslinking proteins in solution one can derive a prediction for the dependence $g_0(c_\times)$, which agrees with experimental observations in fascin-crosslinked actin networks [31]. Similar reasoning has been applied for scruin-crosslinked actin networks using the affine model [32].

The associated low-frequency loss modulus scales linearly with frequency $g'' \sim \omega$ and characterizes the viscous losses of a filament that moves with a velocity $v \sim \omega$ through the solvent. The crossover to the high-frequency regime happens at the frequency scale $\omega_c \sim \kappa/\eta L^4$ with an N-dependent prefactor, set by the plateau modulus and its sensitivity to N.

For high ω there is no coupling from one crosslink to the next. The excited bending modes have small wavelength (see Fig. 4), and perturbations are only local. For high frequencies the Greens function is diagonal,

$$\mathcal{G}_{ij}(\omega) \to \delta_{ij}\frac{1}{\sqrt{8}\kappa^{1/4}(i\omega\eta)^{3/4}}. \tag{16}$$

The $(i\omega)^{3/4}$ scaling can be understood by noticing that, at large ω, each mode in Eq. (14) contributes terms of order $1/\omega$ and the mode spectrum is cut at $q^* \sim \omega^{1/4}$. The determining Eq. (15) is simplified accordingly,

$$1 = \left\langle \sum_i \frac{\cos^2\theta_i}{1 + g^\star \alpha_i \mathcal{G}_{ii}} \right\rangle. \tag{17}$$

This gives $g^\star \sim 1/\mathcal{G} \sim (i\omega)^{3/4}$. The high-frequency scaling is the same as in affine models [4]; however, the prefactor differs by a term l_p/L, which for f-actin is usually not a large number. This factor can, in principle, be changed in experiments; however, care should be taken that by changing, for example, L the network is not changed at the same time (for example, one might freeze in more bents and prestress in networks with longer filaments). Experimentally, the 3/4 scaling is well established and has, for example, been measured with microrheology in Ref. [33].

IV. FINITE CROSSLINK LIFETIME

If thermal fluctuations are comparable to the strength of a crosslink, then the bond will have a finite lifetime. In biological systems the crosslink-induced bonds between filaments usually have a lifetime in the range of seconds. The binding kinetics can therefore be picked up in standard rheological measurements. In fact, some systems display a pronounced peak in the loss modulus g'' at the respective frequencies [34,35]. In the following we explain how crosslink binding and unbinding can be introduced into the theory. Alternative theoretical developments are presented along with the experiments in Refs. [34,35] or, for example, in Refs. [36–38].

We think of the crosslink to live in a one-dimensional periodic energy landscape that represents the binding states along the filament backbone (see Fig. 5). In f-actin the double-helical repeat implies a periodicity of roughly $\delta \approx 50$ nm. While being bound at one site the crosslink stays in the respective minimum of the energy landscape, unbinding corresponds to Kramers escape from this minimum. In the fast-rebinding regime we can assume the crosslink to immediately fall in the neighboring minimum a distance δ away.

Via a force-dependent escape rate $r_\pm = r_0 e^{\pm\beta F\delta}$ one direction is favored over the other. In linear response the crosslink then moves with a velocity $v = F/\zeta$ and friction coefficient $\zeta = k_B T/2r_0\delta^2$, as imposed by the fluctuation dissipation relation and a diffusion constant $D = 2r_0\delta^2$.

We thus conclude that crosslink binding and rebinding processes can be envisioned, on average, as a dash-pot. The friction coefficient is given in terms of microscopic properties of the crosslink and the binding domain of the filament. Each crosslink i may have its own friction coefficient ζ_i, the limit $\zeta_i \to \infty$ representing the case of a nonreversible, i.e., permanently bound ("quenched"), crosslink.

With this insight the response function g on the right-hand side of Eqs. (11) and (12) have to be substituted (in frequency-space) by

$$\bar{g}^{-1} = g^{-1} + (i\omega\zeta)^{-1}, \tag{18}$$

representing a serial connection of crosslink binding domain ζ and viscoelastic medium g (Maxwell element). This modifies Eq. (15) as follows:

$$1 = \left\langle \sum_{ij} (1 + g^\star \Lambda \mathcal{S} G)^{-1}_{ij} \alpha_i \beta_i (\Lambda\beta)_j \right\rangle, \tag{19}$$

the diagonal matrix Λ containing the Maxwell elements of the crosslink, $\Lambda_{ij} = \delta_{ij}\frac{i\omega\zeta_j}{i\omega\zeta_j + g}$.

The result of this modification can be seen in Figs. 6 and 7. Primarily, crosslink binding leads to the appearance of a Maxwell-like peak at small frequencies $\omega^\star \sim g_0/\zeta$, where g_0 is the respective plateau modulus (inset Fig. 6). In Fig. 6 we display the rheology for a mixture of N_r reversible ($\zeta_j \equiv \zeta$)

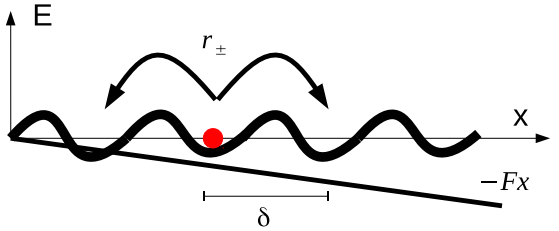

FIG. 5. Binding potential felt by the crosslink taken along the filament axis.

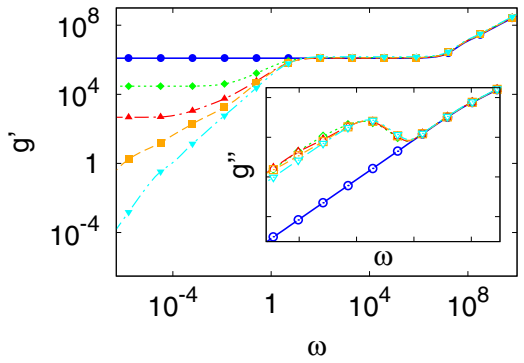

FIG. 6. Storage modulus (main panel) and loss modulus (inset, same axes as in main panel) vs. frequency for different fraction of quenched crosslinks $n_q = N_q/N = 0,0.18,0.2,0.4,1$ (from bottom to top). A second plateau develops when the number of quenched crosslinks is above the percolation threshold. Viscous coefficient of the reversible crosslinks is $\zeta = 10^5$.

and N_q quenched crosslinks ($\zeta_j \to \infty$). If there is a minimum number of quenched crosslinks per filament, then there is a second (lower) plateau modulus at low frequencies. The height of the plateau depends on the number of crosslinks. For frequencies above the Maxwell frequency g_0/ζ all crosslinks are effectively quenched as the network deformation is too fast for the crosslinks to be able to follow. The plateau is therefore determined by the total number of crosslinks. On frequencies far below the Maxwell frequency the reversible crosslinks can be assumed to be removed and only the N_q quenched crosslinks remain. The plateau is therefore determined by only N_q crosslinks. The presence of a plateau at low frequencies indicates that quenched crosslinks are sufficient in number to form a rigid structure—rigidity percolates.

In Fig. 7 we vary the structural randomness of the network. In particular, the distribution $P(\theta)$ of crosslink angles θ is

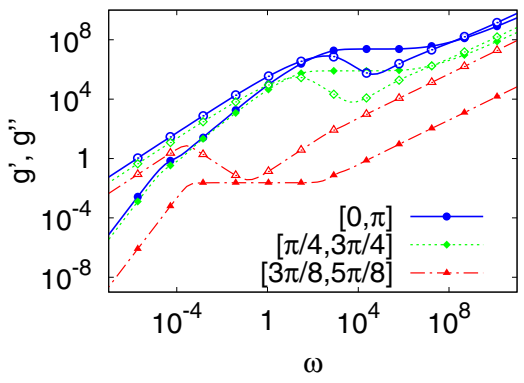

FIG. 7. Frequency-dependent modulus $g^\star = g' + ig''$ for different angular randomness $P(\theta)$ (flat distribution restricted to different intervals as specified in the legend); storage modulus g' (solid lines and filled symbols); loss modulus g'' (broken lines and open symbols). If crosslink intersection angles θ are sufficiently random, then an anomalous regime at small frequencies develops that reflects the spatial inhomogeneity along the single filament.

changed. As a result, a broad intermediate regime develops for the loss modulus whenever the angles are broadly distributed. This regime reflects the spatial heterogeneity along the test filament. The ultimate low-frequency regime ($g'' \sim \omega^2$) is only reached when all crosslinks along the test filament effectively behave equally. The low-frequency behavior in some experiments on f-actin (e.g., Ref. [35]) and also in the simulations of Ref. [16] show a pronounced anomalous tail, $g^\star \sim (i\omega)^{1/2}$, which is explained by Rouse-like relaxation modes. These are not included in the present model.

V. NONLINEAR RESPONSE

A full nonlinear theory has to include several factors, e.g., the reorientation of filaments under large strain [39] or the force-induced change in the polymer end-to-end distance. In addition, the effects of an applied prestress in combination with small amplitude oscillations is an important experimental probe. It is outside the scope of this work to fully combine all these aspects with our theoretical framework. However, progress is possible on a "schematic" level.

A. Prestress

To incorporate a constant prestress in our formalism, we make a "quasilinear" approximation: We assume the linear theory to be valid, while we change the propagator

$$\mathcal{G}_{ij}(\omega) \to \sum_q \frac{\psi_q(x_i)\psi_q^\star(x_j)}{\kappa q^4 + f q^2 + i\omega\eta}, \tag{20}$$

where the new f-dependent term takes care of the reduction of transverse undulations by applying a tensile prestress, adding a term $\sim f(\partial y/\partial s)^2$ to the Hamiltonian [Eq. (1)] or, equivalently, the term $f\partial^2 y/\partial s^2$ to the equation of motion Eq. (11). In essence, this assumes network prestress to act primarily as filament tension. This results in a new stress-dependent plateau modulus $g_f \sim f$, as well as a new regime $g \sim (i\omega)^{1/2}$ at intermediate frequency (see Fig. 8), which is a result of the domination of the fq^2 term and the resulting cutoff of the mode spectrum at $q^* \sim \omega^{1/2}$. The frequency scale for this new regime is $\omega_f \sim f/\lambda^2\eta$, where $\lambda = L/N$ is the wavelength of the relevant bending mode. In order for this

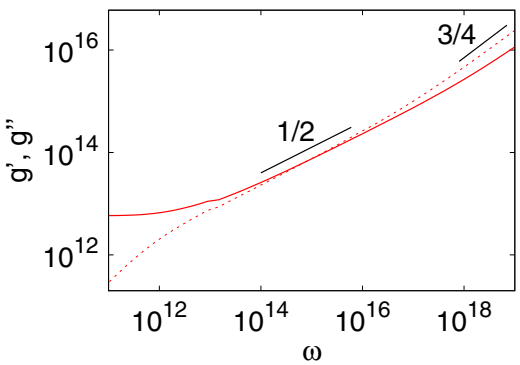

FIG. 8. Modulus vs frequency for a large value of tension ($f/g_0 \approx 10$).

regime to be accessible, the tension needs to be large enough to make $g_f/g_0 > (\omega_f/\omega_0)^{3/4}$, where $\omega_0 \sim \kappa/\lambda^4\eta$ is the relevant frequency scale without tension.

B. Schematic theory for strain ramp

Under large forces, the polymer will no longer behave as inextensible rod. Rather the specific form of the force-extension relation will become important. We can include this factor in a schematic model for the behavior under a strain ramp [40], where the strain linearly increases in time, $\gamma(t) = \dot{\gamma}t$.

This schematic model utilizes the key assumptions of Secs. II–IV: Network strains translate into non-affine filament bending modes via a deformation of the tube; the amplitude of these bends $\bar{y} \sim \gamma L$ grows linearly with strain [see Eq. (3)]; the wavelengths of the bends are slaved to the surrounding network structure [factors $\beta(s)$; see Fig. 4]. The bending wavelengths are thus set by the typical intercrosslink spacing. That is, if we consider a filament with N crosslinks, then the average bending wavelength will be $\lambda = L/N$.

Under larger strain, beyond the linear regime, two processes compete: First, nonlinear filament elasticity (nonlinear force-extension relation) leads to strain-stiffening, and, second, crosslink unbinding leads to an increase in the wavelength of the bending modes and subsequently to strain softening.

For a given bending amplitude $\bar{y}$, an associated longitudinal extension u (increase of end-to-end distance) can be calculated via Pythagoras's law, $u \sim \bar{y}^2/\lambda \sim \gamma^2 L^2/\lambda$.

In response to large elastic deformations the crosslinks start to unbind (neglecting rebinding). Thus, the bending wavelength gets longer, as $\lambda = L/N$, and the elastic energy decreases. The interplay between stiffening and softening is then a competition between elastic stiffening (embodied in the non-linear longitudinal response) and softening via unbinding. To implement the softening part, we need a model for the elastic energy as well as a dynamical evolution equation for the crosslink number $N(t)$. The bending energy of the filament scales $E_b = Nk_\perp \bar{y}^2$ where we have used the bending spring constant $k_\perp \sim \kappa/\lambda^3$ of an elastic filament with bending stiffness κ. For the stretching energy we take the linearized force-extension relation of a wormlike chain with spring constant $k_s \sim \kappa l_p/\lambda^4$ and the persistence length l_p. The total energy then is $E = E_b + E_s$, the force F is the first derivative, and the modulus μ is the second derivative with respect to strain. Without crosslink unbinding, this describes a strain-stiffening system. The strain dependence in the nonlinear regime follows from the longitudinal response and will differ, for example, when one considers an exponential stiffening model as in Ref. [37].

The simplest description for the crosslink dynamics is in terms of a rate equation

$$dN/dt = f(N) - b(N), \tag{21}$$

with forward rate f and backward rate b. Neglecting rebinding, $b = 0$. Unbinding happens at any one of N crosslinks, thus $f = Nk_{\text{off}}$, with an off-rate that may be force dependent, $k_{\text{off}} = k_0 e^{F(N)/F_0}$, with the N-dependent force $F(N)$ as given above. Solving the combined problem then gives Fig. 9. It clearly shows the competition between hardening response as a result of elastic nonlinearities (modulus increases as set by *strain*) and softening response due to crosslink unbinding (modulus decreases as set by *time*). The transition line between both regimes depends on the unbinding rate and agrees well with the results of full network simulations in Ref. [40]. Similar curves have also been found experimentally, for example, in Refs. [40–42].

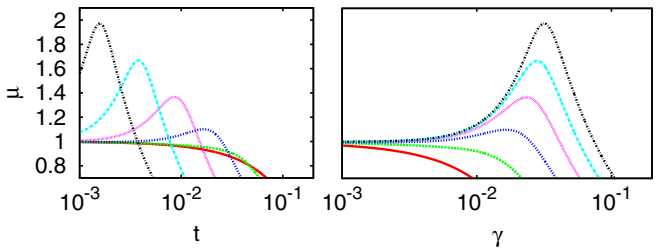

FIG. 9. Nonlinear modulus μ vs time t (left) and vs strain γ (right) for different strain rates. Larger strainrates imply less time for unbinding processes. Therefore more of the elastic nonlinearity is visible in the modulus (the larger the strainrate the higher the peak).

VI. CONCLUSIONS

In conclusion, we have presented a theoretical framework for the linear and nonlinear viscoelastic properties of reversibly connected networks of semiflexible polymers. In our model the network strain does not couple directly to the filament end-to-end distance but rather serves to locally distort the network structure. This induces bending modes in the filaments the amplitude of which grow linearly in strain, and the wavelength of which are slaved to the local network structure, e.g., the distance to the next crosslink, etc. Specifically, we investigated the frequency-dependent linear rheology, in particular in combination with crosslink binding and unbinding processes. At low frequencies the rheology is crosslink dominated and given by an effective Maxwell element, $1/g \sim 1/g_0 + 1/i\zeta\omega$, where $\zeta = k_B T/D$ is the friction coefficient induced by diffusive crosslink un- and rebinding processes. At intermediate frequencies a quasielastic network forms, characterized by a plateau modulus g_0 that sensitively depends on crosslink concentration as well as on network structure. The latter dependence can, for example, be evidenced by monitoring the change of the plateau modulus with changing the typical angles between crosslinked filaments. Finally, at high frequencies we observe a single-filament regime, where the modulus shows scaling with frequency, $g^\star \sim (i\omega)^{3/4}$. The scaling is the same as in affine models; however, the prefactor differs by a factor L/l_p. Going beyond linear response, we devised a schematic model for the nonlinear response in a creep experiment. We found a transition between the hardening and softening responses, as the strainrate or the crosslinker off-rate are tuned. This transition reflects the competition between elastic nonlinearities, which leads to hardening, and crosslink unbinding, which leads to softening and to

network failure. These tests show that our model is capable of reproducing many of the key experimental findings available in the literature.

ACKNOWLEDGMENTS

We acknowledge financial support by the German Science Foundation via the Emmy Noether program (He 6322/1-1) and via SFB 937 (Project No. A16).

APPENDIX

Equation (5) can be solved in a simplified scaling picture. To this end we assume one angle $\theta_i \equiv \theta$, as well as one wavelength, $\lambda = L/N$, to dominate. For a given bending amplitude $y(s) \to y_0$ the Hamiltonian Eq. (1) scales as

$$H_b = \frac{\kappa}{2}\frac{y_0^2}{\lambda^4}L. \tag{A1}$$

The tube potential Eq. (2) can with Eqs. (3) and (4) be written as

$$V = \frac{k_m}{2}\sum_i \alpha_i (y - \beta_i \gamma L)^2. \tag{A2}$$

With the one-angle approximation this scales as

$$V = \frac{k_m}{2} N\alpha (y_0 - \beta\gamma L)^2. \tag{A3}$$

Minimization of $H + V$ with respect to y_0 then yields

$$y_0 = \frac{k_m \alpha}{(\kappa/\lambda^3) + k_m \alpha}\beta\gamma L. \tag{A4}$$

Inserting this into Eq. (5) (dropping the angular average), one finds

$$1 = N\beta^2\alpha\frac{\kappa/\lambda^3}{\kappa/\lambda^3 + k_m\alpha}. \tag{A5}$$

This can be solved for the modulus k_m,

$$k_m = \frac{\kappa}{\lambda^3}\left(N - \frac{1}{\beta^2\alpha}\right)\beta^2, \tag{A6}$$

which is Eq. (6).

[1] A. Bausch and K. Kroy, Nat. Phys. **2**, 231 (2006).
[2] C. P. Broedersz and F. C. MacKintosh, Rev. Mod. Phys. **86**, 995 (2014).
[3] K. Kroy, Curr. Opin. Colloid Interface Sci. **11**, 56 (2006).
[4] F. Gittes and F. C. MacKintosh, Phys. Rev. E **58**, R1241 (1998).
[5] E. Frey, K. Kroy, J. Wilhelm, and E. Sackmann, *Dynamical Networks in Physics and Biology* (Springer, Berlin, 1998), Chap. 9.
[6] D. C. Morse, Phys. Rev. E **63**, 031502 (2001).
[7] J. L. Jones and R. C. Ball, Macromolecules **24**, 6369 (1991).
[8] L. Wolff, P. Fernandez, and K. Kroy, New J. Phys. **12**, 053024 (2010).
[9] C. Heussinger and E. Frey, Phys. Rev. Lett. **97**, 105501 (2006).
[10] R. C. Picu, Soft Matter **7**, 6768 (2011).
[11] J. Wilhelm and E. Frey, Phys. Rev. Lett. **91**, 108103 (2003).
[12] D. A. Head, A. J. Levine, and F. C. MacKintosh, Phys. Rev. E **68**, 061907 (2003).
[13] J. A. Åstrom, P. B. S. Kumar, and M. Karttunen, Soft Matter **5**, 2869 (2009).
[14] P. Müller and J. Kierfeld, Phys. Rev. Lett. **112**, 094303 (2014).
[15] M. Bai, A. R. Missel, W. S. Klug, and A. J. Levine, Soft Matter **7**, 907 (2011).
[16] K. W. Müller, R. F. Bruinsma, O. Lieleg, A. R. Bausch, W. A. Wall, and A. J. Levine, Phys. Rev. Lett. **112**, 238102 (2014).
[17] F. C. MacKintosh, J. Käs, and P. A. Janmey, Phys. Rev. Lett. **75**, 4425 (1995).
[18] C. Storm, J. J. Pastore, F. C. MacKintosh, T. C. Lubensky, and P. A. Janmey, Nature **435**, 191 (2005).
[19] K. Kroy and J. Glaser, New J. Phys. **9**, 416 (2007).
[20] M. Das, D. A. Quint, and J. M. Schwarz, PLoS One **7**, e35939 (2012).
[21] X. Mao, O. Stenull, and T. C. Lubensky, Phys. Rev. E **87**, 042601 (2013).
[22] M. Sheinman, C. P. Broedersz, and F. C. MacKintosh, Phys. Rev. E **85**, 021801 (2012).
[23] C. P. Broedersz, X. Mao, T. C. Lubensky, and F. C. MacKintosh, Nat. Phys. **7**, 983 (2011).
[24] A. J. Liu, S. R. Nagel, W. van Saarloos, and M. Wyart, *The Jamming Scenario—An Introduction and Outlook* (Oxford University Press, Oxford, 2010), Chap. 9.
[25] C. Heussinger, B. Schaefer, and E. Frey, Phys. Rev. E **76**, 031906 (2007).
[26] C. Heussinger and E. Frey, Eur. Phys. J. E **24**, 47 (2007).
[27] C. P. Broedersz, M. Sheinman, and F. C. MacKintosh, Phys. Rev. Lett. **108**, 078102 (2012).
[28] E. M. Huisman, C. Heussinger, C. Storm, and G. T. Barkema, Phys. Rev. Lett. **105**, 118101 (2010).
[29] E. M. Huisman and T. C. Lubensky, Phys. Rev. Lett. **106**, 088301 (2011).
[30] D. A. Head, A. J. Levine, and F. C. MacKintosh, Phys. Rev. Lett. **91**, 108102 (2003).
[31] O. Lieleg, M. M. A. E. Claessens, C. Heussinger, E. Frey, and A. R. Bausch, Phys. Rev. Lett. **99**, 088102 (2007).
[32] J. H. Shin, M. L. Gardel, L. Mahadevan, P. Matsudaira, and D. A. Weitz, Proc. Natl. Acad. Sci. USA **101**, 9636 (2004).
[33] G. H. Koenderink, M. Atakhorrami, F. C. MacKintosh, and C. F. Schmidt, Phys. Rev. Lett. **96**, 138307 (2006).
[34] O. Lieleg, M. M. A. E. Claessens, Y. Luan, and A. R. Bausch, Phys. Rev. Lett. **101**, 108101 (2008).

[35] C. P. Broedersz, M. Depken, N. Y. Yao, M. R. Pollak, D. A. Weitz, and F. C. MacKintosh, Phys. Rev. Lett. **105**, 238101 (2010).
[36] C. Vaca, R. Shlomovitz, Y. Yang, M. T. Valentine, and A. J. Levine, Soft Matter **11**, 4899 (2015).
[37] L. Wolff and K. Kroy, Phys. Rev. E **86**, 040901 (2012).
[38] C. Heussinger, New J. Phys. **14**, 095029 (2012).
[39] H. E. Amuasi, C. Heussinger, R. L. C. Vink, and A. Zippelius, New J. Phys. **17**, 083035 (2015).
[40] M. Maier, K. Müller, C. Heussinger, S. Köhler, W. Wall, A. Bausch, and O. Lieleg, Eur. Phys. J. E **38**, 50 (2015).
[41] O. Lieleg, M. M. A. E. Claessens, and A. R. Bausch, Soft Matter **6**, 218 (2010).
[42] C. Semmrich, T. Storz, J. Glaser, R. Merkel, A. R. Bausch, and K. Kroy, Proc. Natl. Acad. Sci. USA **104**, 20199 (2007).